GEO-HAZARDS STUDIES BY PALSAR INTERFEROMETRY

PI No: 390
Xiaoli Ding [1], Lei Zhang[1], Guangcai Feng[1], Mi Jiang[1], and Jun Hu[2],

[1] The Hong Kong Polytechnic University, Hung Hom, KLN, Hong Kong
[2] Central South University, Changsha, China

1. INTRODUCTION

As an L-band space-borne SAR sensor, ALOS/PALSAR has been playing a crucial role in globally assessing natural hazards such as earthquakes, volcanoes, glaciers and urban land subsidence. Geophysical research has benefited enormously from the use of ALOS/PALSAR observations. This report summaries the work performed by HKPolyU/LSGI InSAR group using the PALSAR data.

2. COSEISMIC DISPLACEMENT

ALOS/PALSAR's all-weather, day and night imaging and vegetation penetration capabilities coupled with the high detectable deformation gradients make it a fundamental instrument for coseismic displacement monitoring. Several devastated earthquakes in recent years have been successfully observed by ALOS/PALSAR. With the data provided by JAXA, HKPolyU/LSGI InSAR group mapped a set of coseismic displacement fields associated with earthquakes such as the 2011 Mw 9.0 Tohoku-Oki earthquake, 2010 Mw 7.1 Darfield earthquake, 2010 Mw 7.1 Yushu earthquake, and 2008 Mw 8.0 Wenchuan earthquake. During the data processing the conventional InSAR techniques together with approaches for correcting the orbital ramps have been applied to achieve useful results.

A. Tohoku-Oki Earthquake

On 11 March 2011, a magnitude Mw 9.0 earthquake occurred near the northeastern coast of Honshu, Japan (38.322°N, 142.369°E) followed by a destructive tsunami (waves up to 37.9m). The earthquake was preceded by a series of large foreshocks over a period of two days which began on 9 March with an Mw 7.3 event approximately 40 km from the hypocenter of the March 11 earthquake and followed by hundreds of aftershocks above Mw4 in the following two months. The coseismic displacement of the quake has been measured by both GPS stations and InSAR. However the released displacement maps from different teams and groups are inconsistent with each other partially due to the distortion of orbital errors (Fig. 1(a)). In addition, the precision of InSAR measurements needs validated also. Our work lies in two-fold, i.e., orbital ramp correction and quantitative comparison between InSAR and GPS observations.

Table 1 ALOS/PALSAR acquisitionsused for coseismicdeformation mapping

Track	Frames	Master	Slave	Days after quake	Perp. baseline (m)	Pass
400	790-800	11 Jan. 2011	13 Apr. 2011	33	1112	A
401	760-800	28 Oct. 2010	15 Mar. 2011	4	1457	A
402	760-800	29 Sep. 2010	1 Apr. 2011	21	1194	A
403	730-800	3 Mar. 2011	18 Apr. 2011	38	354	A
404	700-770	2 Feb. 2011	20 Mar. 2011	9	831	A
405	690-750	19 Feb. 2011	6 Apr. 2011	26	402	A

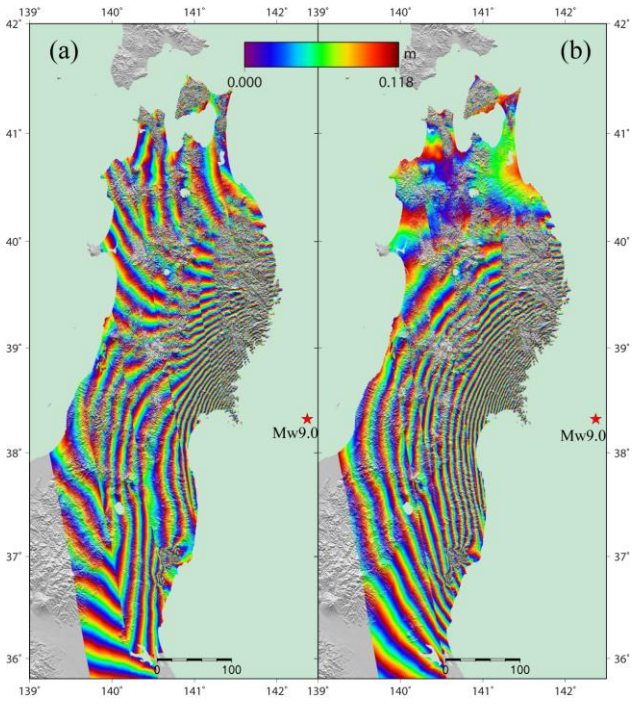

Fig.1 Coseismic deformation of the Tohoku-Oki earthquake measured by PALSAR acquisitions before (a) and after (b) orbital ramps correction. Each color cycle represents 11.8 cm of LOS displacement toward or away from the satellite.

The SAR data (see Table 1) were processed from raw products with conventional two-pass differential interferometry. During the SAR data processing, the preliminary orbit delivered with the PALSAR acquisitions

was used. All the FBD PALSAR data are oversampled to the resolution as FBS mode. The 90m SRTM v4.1 were used to remove the phase component contributed by the topography. We applied a multi-look operation (10×30) for PALSAR in range and azimuth direction before phase unwrapping. We use the minimum cost flow algorithm (MCF) to unwrap each of the interferograms, which minimizes the phase jump errors and simultaneously maximizes the availability of InSAR phases [1]. Because the reference points for each interferogram are different in phase unwrapping, we calibrated the displacement using the distributed GPS observations throughout the interferogram at each track. In order to illustrate the finer structure of the displacement field, we rewrap the displacement with the same fringe cycle of 11.8 cm along the LOS direction in PALSAR and ASAR displacement products. Figure 1a shows the wrapped displacement from 6 ascending PALSAR tracks where orbital ramps are clearly visible.

Thanks to the dense GPS network, abundant GPS measurements allowed us to remove the orbital ramps from interferograms reliably. After the projection of GPS observations into the radar line of sight (LOS) direction, a 2D polynomial was employed to fit the discrepancies between GPS derived coseismic displacement and the InSAR measurements of their nearest pixels. The coherence of pixels was used as a weight matrix in this 2-D quadratic fitting. The points with large residuals (above 3 times of the RMS) were excluded to avoid the phase unwrapping errors and the local effects on some GPS stations. The corrected displacement field associated with this event was rewrapped and shown in Fig.1 (b). It is clear that the displacement pattern has changed significantly. After the orbital ramp correction, the root mean square (RMS) of misfits between GPS and InSAR measurements has reduced at every track and the average RMS decreased from 15.6 cm to 7.2 cm. The corrected interferograms show dense fringes raised by this event, corresponding to up to 3.7 m LOS displacement.

The GPS measurements only provided point displacements in north, east and vertical directions, while InSAR can provide a continuous field of displacement in radar LOS direction. The GEONET network of Japan, consisting of 1224 GPS stations spaced ~ 20 km apart, allows computation of regular grids of the north, east and vertical components of the displacement. We first interpolated each component and then produced the synthetic LOS maps. By differencing the corrected coseismic deformation in Figure 1(b) with the synthetic coseismic deformation, we got the residual map between the InSAR and GPS measurements (Fig.2). It can be found that the aftershock displacements have been successfully isolated, which are due to a series of shallow aftershocks with magnitudes of Mw5.3~6.1 and Mw6.6 on 2011/04/11 occurred in western Iwaki (see Figure 2(c)) and two Mw5.3-6.1 aftershocks on 2011/03/19 that occurred in northern Hitachi (Fig.2(d)) .

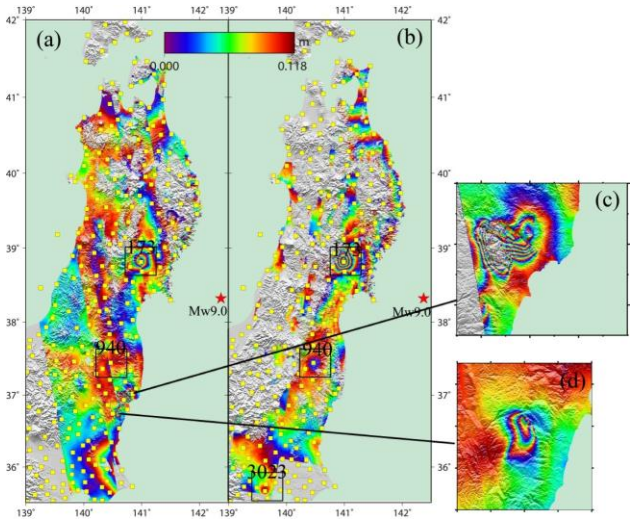

Fig.2 Residual maps between the InSAR and interpolated GPS measurements. Decorrelated regions of the interferograms are masked out. The yellow squares indicate GPS station locations. (a) Residual map of ALOS/PALSAR measurement; (b)Residual map of Envisat/ASAR measurement; (c) and (d) The aftershock deformation. The black squares locate the GPS stations (0173, 940 and 3023) with local station effect.

B. Darfiled Earthquake

At 16:35:46 (UTC) on 3 September 2010, a huge earthquake with a magnitude of Mw 7.1 struck the town of Darfield in the South land of New Zealand. The epicenter was 40 kilometers west from the second largest city of the Island, Christchurch. The main shock and subsequent aftershocks had caused widespread and serious damages to infrastructure and residential houses throughout the region, particularly in the urban area of Christchurch. Soon after the ALOS/PALSAR data (see Table 2) were available, we performed the conventional 2-pass DInSAR on them to get the LOS coseismic displacement along both the ascending and descending tracks.

Table 2. The PALSAR data used in this event

	Track	Frame	Acquisition time before the main shock	Acquisition time after the main shock	Temporal coverage (d)	Perpendicular baseline (m)
Ascending	337	629,630,631	11:57 (UTC) 2008-02-05	11:57 (UTC) 2010-09-28	966	-216
Descending	631	450,451,452	22:01 (UTC) 2008-07-22	22:04 (UTC) 2010-09-12	782	-2639

The SRTM DEM was used to eliminate the topographic effect in the interferograms. Before phase unwrapping, the interferograms were filtered by the improved Goldstein filter [2] to suppress phase noise. The long wavelength signals, including orbit errors and possible atmospheric effects, have been modeled and eliminated from the

interferograms by a biquadratic polynomial. The LOS displacement is shown in Figure 2, which had been rewrapped for better visual effect. Several fringes are clearly visible in the area of Darfield in both ascending and descending measurements. It is also observed that decorrelation is serious near the epicenter, which is believed due to the excessive ground motion in this region.

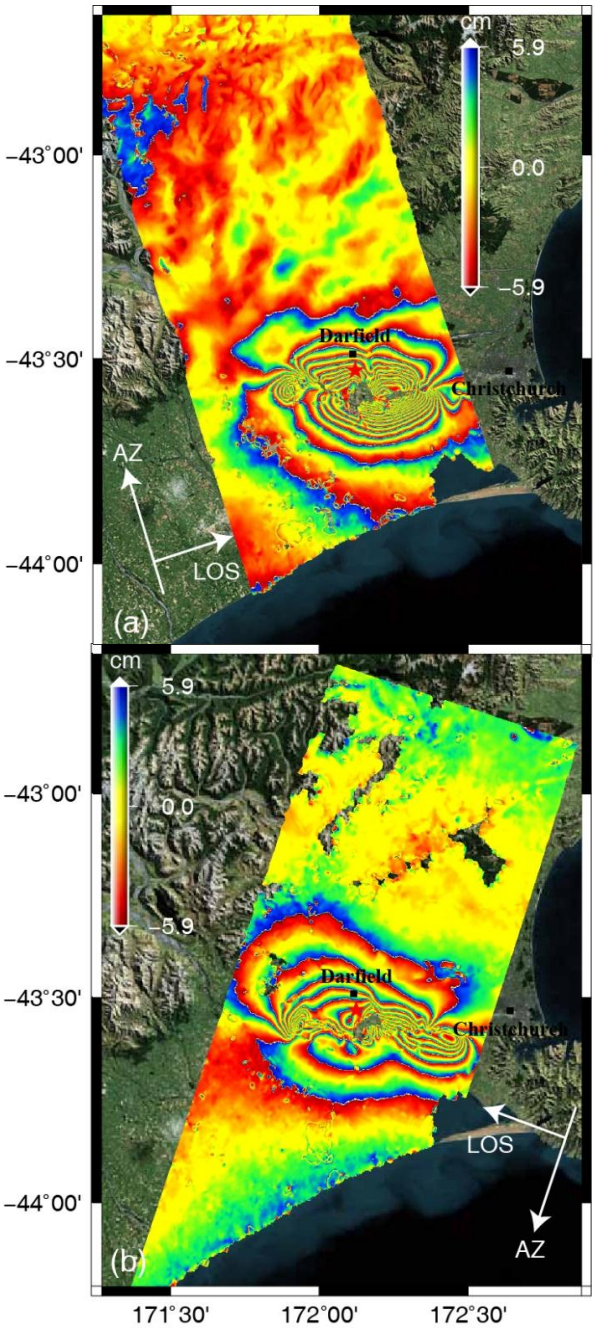

Fig.2. The LOS coseismic displacement fields along ascending (a) and descending tracks (b)

C. Yushu Earthquake

On 20 April 2010, a magnitude Mw 7.8 earthquake struck Yushu County, Qinghai province of China. The quake occurred at one of the most active fault zones in eastern Tibet. To determine the coseismic displacement, we performed the 2-pass DInSAR processing on a pair of ALOS/PALSAR data. The phase component contributed by topography was removed using the SRTM DEM with a spatial resolution of 90 m. The SNAPHU algorithm was employed to unwrap the interferogram and a 2D polynomial is used to remove the orbital error related phases. The rewrapped coseismic displacement is shown in Fig. 3.

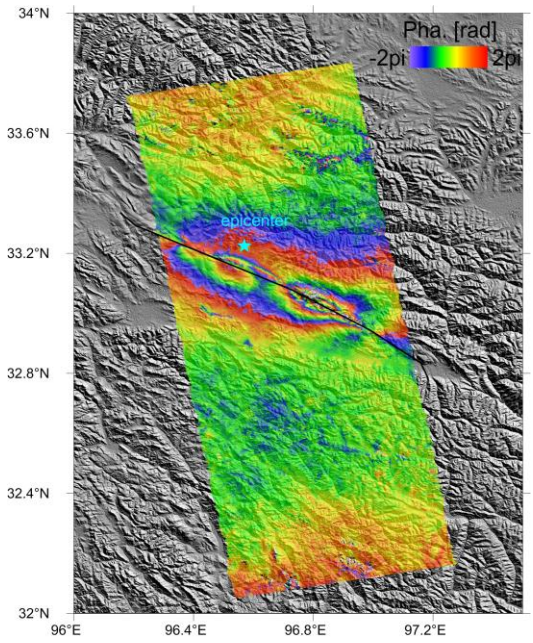

Fig.3 The coseismic displacement of Yushu earthquake determined from ALOS/PALSAR data

D. Wenchuan Earthquake

On 12 May 2008, Mw 7.9 Wenchuan earthquake struck the eastern edge of the Tibetan plateau and devastated cities along the northwest margin of the Sichuan basin, causing more than 80000 dead and 380,000 injured. We use L-band ALOS/PALSAR data from six ascending tracks 471 to 476, to form interferograms of coseismic deformation in regions that cover the Longmen Shan fault zone and the rupture of the Wenchuan earthquake. L-band SAR has the advantage that it experiences less temporal decorrelation in heavily vegetated areas due to its ability to penetrate vegetation. The ALOS/PALSAR radar incidence angle is approximately 38.7° from vertical, so the measurements are slightly more sensitive to horizontal ground displacement than either ERS or ENVISAT, which have ~ 23° incidence angle.

The coseismic displacement associated with this event is shown in Fig. 4 where pairs without ionospheric effects were used [3].

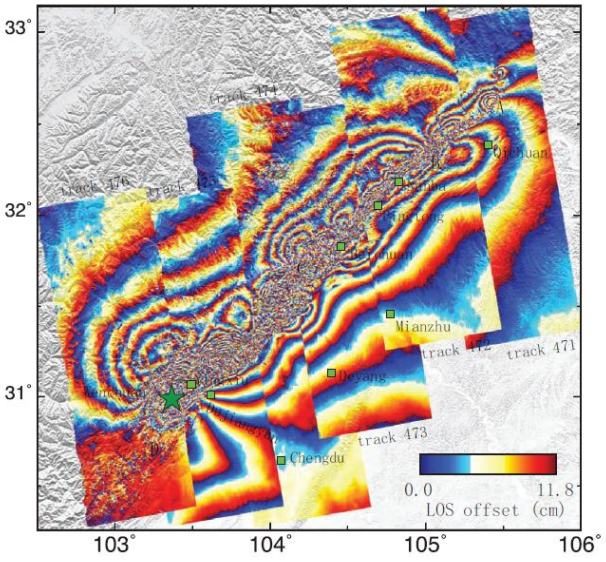

Fig. 4 Interferogram of coseismic deformations of the Wenchuan earthquake. Six tracks (from Track 471 to Track 476) of ALOS/PALSAR data without ionospheric perturbation were used to generate the interferogram of coseismic deformations.

From the processing a set of coseismic L-band SAR data, we noticed that orbital errors commonly exist in the interferograms and a low order polynomial had to be used to remove these orbital error patterns. In addition, the ionospheric effect of ALOS/PALSAR data had gained more and more attention and possible correction methods have also been proposed. By analyzing azimuth offset maps of image pairs over seismic regions, we find that many of them are distorted by ionospheric effects, which makes us suspect whether the abnormal ionosphere has a strong relationship with the occurrence of earthquakes. In the future work we plan to collect more data to explore possible clues.

3. LINEAR INFRASTRUCTURE MONITORING

Reliably monitoring of long-term deformation of flexible structures such as large-scale bridges to assess the structural safety is vitally important. We experimented to use ALOS/PALSAR data to monitor the deformation of Donghai Bridge, the second longest cross-sea bridge in the world having a total length of 32.5km. Since the bridge located in the north of Hangzhou Bay in the East China Sea, accurately coregistering the images is a challenging task. The proposed method termed temporarily coherent point (TCP) SAR interferometry (InSAR)[5][6] can identify and extract TCPs between two SAR acquisitions based on the spatial characteristics of offsets in both the range and azimuth directions. Coregistration is then performed using the offsets of these TCPs, resulting in high-quality interferometric phases. By the TCPInSAR method the deformation rate along the bridge can be estimated from the wrapped phases with no need of phase unwrapping. The achieved results indicate that the bridge suffered a largest line-of-sight deformation up to 1.2 cm from January 2009 to July 2009 at the cable-stayed part [4].

A. Data selection

Over the Donghai Bridge we have two kinds of radar data at hand, i.e., the Envisat ASAR data and ALOS PALSAR data. However the C-band ASAR data are so noisy in the study area that it is hard to extract any useful information. In contrast the L-band PALSAR data which were acquired under Fine Beam Double Polarization (FBD) mode appear to be very “sharp” (Fig. 5). When we looked into the PALSAR data we further found that the HV polarized data (Figure 5b) have better performance on minimizing the “ghost” (called ambiguity in general) in the sea area and suppressing the side lobe effects on the island than the HH polarized data (Figure 5a). Hence we finally chose the HV PALSAR data as observations to determine the long-term deformation rate of the Donghai Bridge. From the 6 interferograms generated by the 4 images we selected 3 independent ones with relatively short baselines for our least squares model.

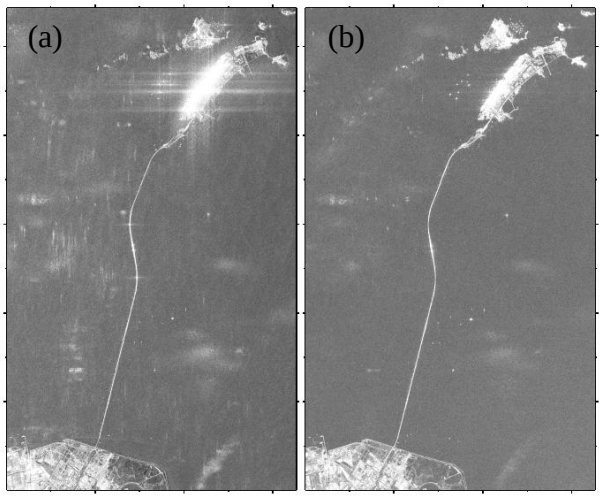

Fig. 5 An example of the ALOS/PALSAR data over Donghai Bridge. (a) HH polarization; (b) HV polarization

B. Temporarily Coherent Point selection

Temporarily coherent points (TCP) are the points in the interferograms that keep coherent during one or several intervals of SAR acquisitions but it is not necessary to be visible in the whole time span. We identify these points

primarily based on the spatial characteristics of offset consistency in range and azimuth directions. The theoretical analysis and real data test of the method can be found [5].

C. TCP coregistration

Coregistration of SAR images is the first and vital step in the InSAR processing chain. However the fact that long cross-sea bridges are usually surrounded by sea area poses a great challenge to conventional coregistration method which employs distributed windows over the whole image to estimate the offsets between corresponding pixels. Since the large portion of pixels located in the sea, the offsets estimated from these pixels are not stable and vary randomly according to the changing window sizes although their SNR appear to be higher than the threshold. In order to overcome the distortions on the coherent points caused by conventional coregistration method, we determine the offset polynomial for resampling slave images only from the offsets at these coherent points only.

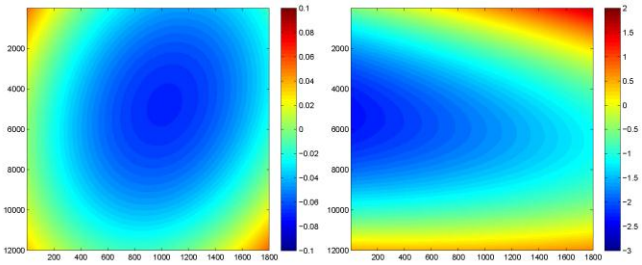

Fig. 6 The difference of offset polynomials along range (left) and azimuth directions (right) determined from distributed windows and TCPs respectively

Fig. 6 shows the differences between global polynomial and TCP polynomial, indicating that in this case the global polynomial introduced more bias in azimuth direction.

D. Least Squares Model

In areas undergoing gentle deformation it is found that for the multi-master interferograms with short baselines, there is usually no phase ambiguity at most arcs constructed by two nearby points since the double-differential phase components contributed by topography errors and atmospheric artifacts appear to be very low. In addition, connection using local Delaunay triangulation ensures the relative rate between two connected points to be small. The model we proposed takes arcs without ambiguities as observations for estimating the DEM errors and deformation rates based on the least squares. Here we just recall the model briefly. The details of the model can be found in [5]. Suppose that N differential interferograms with temporal baselines of ti (i=1, 2, …, N) have been generated from a set of M SAR images over the study area. For an arc formed by connecting TCP A and TCP B, N observation equations can be written with the N interferometric pairs as follows

$$\begin{cases} \Delta\Phi(x,y,t_1) = \partial(x,t_1)\cdot\Delta h_{x,y} + \beta(t_1)\cdot\Delta v^1_{x,y} + \Delta\omega(x,y,t_1) \\ \Delta\Phi(x,y,t_2) = \partial(x,t_2)\cdot\Delta h_{x,y} + \beta(t_2)\cdot\Delta v^2_{x,y} + \Delta\omega(x,y,t_2) \\ \cdots \\ \Delta\Phi(x,y,t_N) = \partial(x,t_N)\cdot\Delta h_{x,y} + \beta(t_N)\cdot\Delta v^N_{x,y} + \Delta\omega(x,y,t_N) \end{cases} \quad (1)$$

Where $\partial(x,t_i)$ is the conversion factor for the differential elevation error ($\Delta h_{x,y}$), $\beta(t_i)$ is the conversion factor for the relative deformation rate ($\Delta v^i_{x,y}$) and $\omega(x,y,t_i)$ is the differential part of phase components related to atmospheric delay and other noise. The differential deformation rates of the arc for all the temporal baselines can be treated as either constant or nonconstant, i.e.,

$$\boldsymbol{\Delta V}_{x,y} = \left[\Delta v^1_{x,y} \quad \Delta v^2_{x,y} \quad \cdots \quad \Delta v^N_{x,y}\right]^T \quad (2)$$

where $\Delta v^i_{x,y}$ stands for the differential rate related to the ith interferometric pair with temporal baseline t_i. The equations (2) can be rewritten in the matrix form as follows,

$$\boldsymbol{\Delta\Phi} = \boldsymbol{A}\begin{bmatrix}\Delta h_{x,y} \\ \boldsymbol{\Delta V}_{x,y}\end{bmatrix} + \boldsymbol{W} \quad (3)$$

where

$$\boldsymbol{\Delta\Phi} = \left[\Delta\Phi(x,y,t_1) \quad \Delta\Phi(x,y,t_2) \quad \cdots \quad \Delta\Phi(x,y,t_N)\right]^T \quad (4)$$

$$\boldsymbol{W} = \left[\Delta\omega(x,y,t_1) \quad \Delta\omega(x,y,t_2) \quad \cdots \quad \Delta\omega(x,y,t_N)\right]^T \quad (5)$$

$$\boldsymbol{A} = \begin{bmatrix}\partial(x,t_1) & \partial(x,t_2) & \ldots & \partial(x,t_N) \\ \beta(t_1) & \beta(t_2) & \ldots & \beta(t_N)\end{bmatrix}^T \quad (6)$$

The unknown parameters $\hat{\boldsymbol{X}}$ can be solved by the LS approach, which can be expressed by

$$\hat{\boldsymbol{X}} = \begin{bmatrix}\Delta\hat{h}_{x,y} \\ \hat{\boldsymbol{\Delta V}}_{x,y}\end{bmatrix} = \left(\boldsymbol{A}^T\boldsymbol{P}^{dd}\boldsymbol{A}\right)^{-1}\boldsymbol{A}^T\boldsymbol{P}^{dd}\boldsymbol{\Delta\Phi} \quad (7)$$

where $\hat{}$ denotes the estimated quantities, and $\boldsymbol{P}^{dd}$ is the prior weight matrix which can be obtained by taking the inverse of the variance matrix of the double-difference phases. It is worth noting that when in the real case the matrix $\boldsymbol{A}^T\boldsymbol{P}^{dd}\boldsymbol{A}$ happens to be singular, a pseudoinverse of the matrix obtained by singular value decomposition (SVD) is used instead, i.e., $\left(\boldsymbol{A}^T\boldsymbol{P}^{dd}\boldsymbol{A}\right)^{-1} = \left(\boldsymbol{A}^T\boldsymbol{P}^{dd}\boldsymbol{A}\right)^{+}$. The estimated quantities for $\boldsymbol{\Delta\Phi}$ can be derived by

$$\hat{\boldsymbol{X}} = \begin{bmatrix}\Delta\hat{h}_{x,y} \\ \hat{\boldsymbol{\Delta V}}_{x,y}\end{bmatrix} = \left(\boldsymbol{A}^T\boldsymbol{P}^{dd}\boldsymbol{A}\right)^{-1}\boldsymbol{A}^T\boldsymbol{P}^{dd}\boldsymbol{\Delta\Phi} \quad (8)$$

The residuals of the measurements can be derived by

$$\begin{aligned} \boldsymbol{Q}_{\hat{x}\hat{x}} &= \left(\boldsymbol{A}^T\boldsymbol{P}^{dd}\boldsymbol{A}\right)^{-1} \\ \boldsymbol{Q}_{\Delta\hat{\Phi}\Delta\hat{\Phi}} &= \boldsymbol{A}\left(\boldsymbol{A}^T\boldsymbol{P}^{dd}\boldsymbol{A}\right)^{-1}\boldsymbol{A}^T \\ \boldsymbol{Q}_{rr} &= \boldsymbol{Q}^{dd} - \boldsymbol{A}\left(\boldsymbol{A}^T\boldsymbol{P}^{dd}\boldsymbol{A}\right)^{-1}\boldsymbol{A}^T \end{aligned} \quad (9)$$

After the LS solution for each arc, the outlier detector proposed by Zhang et al. [6] is applied to check if the phase measurements for the arc have phase ambiguities. Both the LS residuals and variance components for the arc are used for such quality check. For subsequent analysis,

the unacceptable arcs should be discarded. After deriving the parameters (i.e., elevation-error and deformation-rate increments) of all the valid arcs, we can determine the parameters (i.e., elevation errors and deformation rates) in absolute sense of all the valid TCPs by a spatial integration method with a given reference point [6].

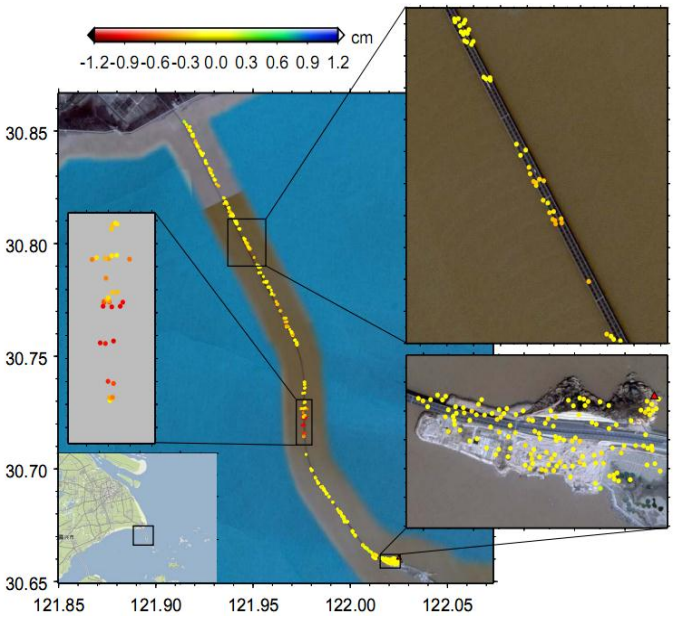

Fig. 7 Deformation rate of TCPs along the bridge

E. Results

The least squares estimation of deformation rate of the identified TCP is shown in Fig. 7. The reference point was selected at an island which assumed to be stable. The largest deformation rate appeared on a cable-stayed bridge over the main navigation channel, up to 2.3cm/y. The cable-stayed bridge is known as a temperature sensitive structure. The difference in temperature of cable and beam will influence the cable force and elevation of the main beam. Although there are no published results on the temperature effects on the Donghai Bridge especially the cable-stayed section, the studies on similar bridges show that the changes of elevation caused by the variation of temperature are up to several centimetres. The PALSAR used were acquired at 10:23 pm local time in January, February, April and July respectively and the mean night-time temperature in those months were 1℃, 1℃, 10℃ and 23℃. It can be concluded that the large deformation rate on the cable-stayed bridge are mainly caused by the temperature changes. It should be also noted that in other parts of the bridge there are also some relatively large deformation rates. Since the bridge is located in a very rough sea environment it suffers many serious effects, such as the seasonal winds, the tide, and foundation settlement. We need to collect more environmental materials and collaborate with the bridge engineers to draw a reliable conclusion on the safety of the bridge.

4. SUMMARY

With the ALOS/PALSAR data provided by JAXA, HKPolyU/LSGI InSAR group has performed a set of projects, including the determination of coseismic displacements associated with several huge earthquakes and long-cross sea bridge monitoring. Thanks to the excellent features of the L-band SAR data, such as vegetation penetration ability and relatively high spatial resolution, encouraging results have been successfully achieved from these projects, which improved our understanding of the seismic mechanisms and the interaction between man-made infrastructures and natural forces (such as temperature load, wind load, and tide load) .

5. ACKNOWLEDGEMENT

We are grateful to JAXA for the supply of the ALOS/PALSAR data.

6. REFERENCES

[1] C.W., Chen, and H. A., Zebker, Two-dimensional phase unwrapping with use of statistical models for cost functions in nonlinear optimization, J. Opt. Soc. Am. A., 18(3), 338-351, 2001.

[2] Z.W.,Li, X.L., Ding, C., Huang, D.W., Zheng, W.B., Zou, Y.K., Shea, Filtering method for SAR interferograms with strong noise. Int. J. Remote Sens., 27(4), 2991-3000, 2006.

[3]G.C., Feng, E. Hetland, X.L., Ding, Z.W., Li, and L. Zhang, Coseismic fault slip of the 2008 Mw 7.9 Wenchuan earthquake estimated from InSAR and GPS measurements, Geophys. Res. Lett., 37, L01, 302, 2010.

[4] L., Zhang, X.L., Ding, and Z., Lu, Study of bridge deformation by temporarily coherent points between multiple SAR acquisitions, International Workshop on Spatial Information Technologies for Monitoring the Deformation of Large-Scale Man-made Linear Feature, Hong Kong, 2010.

[5] L., Zhang, X.L., Ding, and Z., Lu, Ground settlement monitoring based on temporarily coherent points between two SAR acquisitions, ISPRS J Photogramm., 66(1), 146-152, 2011.

[6] L., Zhang, X.L., Ding, and Z., Lu, Modeling PSInSAR time series without phase unwrapping, IEEE Trans. Geosci. Remote Sens., 49(1), 547-556, 2011.